DNA Nanotechnology

International Edition: DOI: 10.1002/anie.201811746
German Edition: DOI: 10.1002/ange.201811746

Quantitative Mapping of Endosomal DNA Processing by Single Molecule Counting

Ved Prakash, Konstantinos Tsekouras, Muthukumaran Venkatachalapathy, Laurie Heinicke, Steve Pressé, Nils G. Walter, and Yamuna Krishnan**

Abstract: *Extracellular DNA is engulfed by innate immune cells and digested by endosomal DNase II to generate an immune response. Quantitative information on endosomal stage-specific cargo processing is a critical parameter to predict and model the innate immune response. Biochemical assays quantify endosomal processing but lack organelle-specific information, while fluorescence microscopy has provided the latter without the former. Herein, we report a single molecule counting method based on fluorescence imaging that quantitatively maps endosomal processing of cargo DNA in innate immune cells with organelle-specific resolution. Our studies reveal that endosomal DNA degradation occurs mainly in lysosomes and is negligible in late endosomes. This method can be used to study cargo processing in diverse endocytic pathways and measure stage-specific activity of processing factors in endosomes.*

Macrophages are innate immune cells that endocytose single- and double-stranded DNA through scavenger receptors. Endocytosed DNA cargo is trafficked along the endolysosomal pathway, progressing from the early endosome to the late endosome, finally reaching the lysosome where it is degraded. The stage-specific processing of endocytic cargo has important implications for pathogen evasion of the immune system, antigen cross-presentation, as well as in differentiating "self" i.e., molecules of host origin, and non-self, i.e., molecules of foreign or pathogenic origin.[1–3] DNA is distinguished as self or non-self by host immune cells based on their relative rates of digestion in endocytic organelles.[2] Immunogenic CpG-containing DNA (CpG-DNA) is processed in endolysosomes of dendritic cells by DNase II such that the digestion-resistant DNA fragments activate Toll-like receptor-9 (TLR-9).[4] However, it is still unclear in which organelle these processes occur owing to the paucity of quantitative assays in cargo processing while retaining organelle-specific localization information. Endosomal processing is mainly studied using biochemical assays such as sulfation, radio labeling, RT-PCR, and transient or induced protein expression.[5–8] While these methods quantitate cargo processing in cell extracts, organelle-specific spatial information cannot be obtained. In contrast, fluorescence microscopy provides organelle-specific spatial information but without the ability to quantitate endocytosed cargo.[5,9,11,12] Although super-resolution microscopy has been used to quantitate marker proteins in organelles,[13,14] one still cannot quantitatively map the processing of endocytic cargo.

Herein, we have developed a method to count endosomal cargo by photobleaching upon targeting fluorescently labeled DNA to specific subcellular compartments.[15] Photobleaching has been used to count cytosolic microRNA copy number.[16] Herein, we expand this concept to include organelle-specific information and thereby address cargo processing by developing a method called organellar single-molecule, high-resolution localization and counting (oSHiRLoC). Using oSHiRLoC, we combine the molecular precision afforded by synthetic DNA reporters, spatial information provided by fluorescence microscopy, and the quantitative information yielded by photobleaching-based counting to map the DNase II-mediated DNA processing along the endolysosomal pathway.

In order to construct organelle specific maps of endosomal DNA processing, we incubated (a "pulse" step) alveolar macrophages J774A.1 cells with a 57-base pair double-stranded (ds)DNA reporter cargo labeled with Alexa 488 (dsDNA-A488) in 19 mole equivalents excess of a reference tracer, i.e., the same dsDNA sequence labeled with Cy5 fluorophore (dsDNA-Cy5) (Figure 1a). These sequences were chosen based on previously reported sensors from our lab for the detection of various analytes.[17–20] Cells were washed, incubated for a specified duration (a "chase" step), fixed and imaged using total internal reflection fluorescence (TIRF) microscopy. The brighter, more photostable Alexa488 channel was used as a fiducial marker of the endocytic compartment; while the Cy5 channel was used to generate photobleaching reporter time traces, leveraging the low cellular autofluorescence in this channel (Figure 1b). Given the TIRF penetration depth of circa 250 nm, approximately 52% of early endosomes ($n = 6$ cells), 37% of late

[*] Dr. L. Heinicke, Prof. N. G. Walter
Single Molecule Analysis Group, Department of Chemistry
University of Michigan
Ann Arbor, MI 48109-1055 (USA)
E-mail: nwalter@umich.edu
Dr. V. Prakash, Dr. M. Venkatachalapathy, Prof. Y. Krishnan
Department of Chemistry, University of Chicago
Chicago, IL 60637 (USA)
E-mail: yamuna@uchicago.edu
Prof. Y. Krishnan
Grossman Institute of Neuroscience, Quantitative Biology and Human Behavior, University of Chicago
Chicago, IL 60637 (USA)
Dr. K. Tsekouras, Prof. S. Pressé
Department of Physics and School of Molecular Sciences
Arizona State University
Tempe, AZ 85287 (USA)
Supporting information and the ORCID identification number(s) for the author(s) of this article can be found under: https://doi.org/10.1002/anie.201811746.

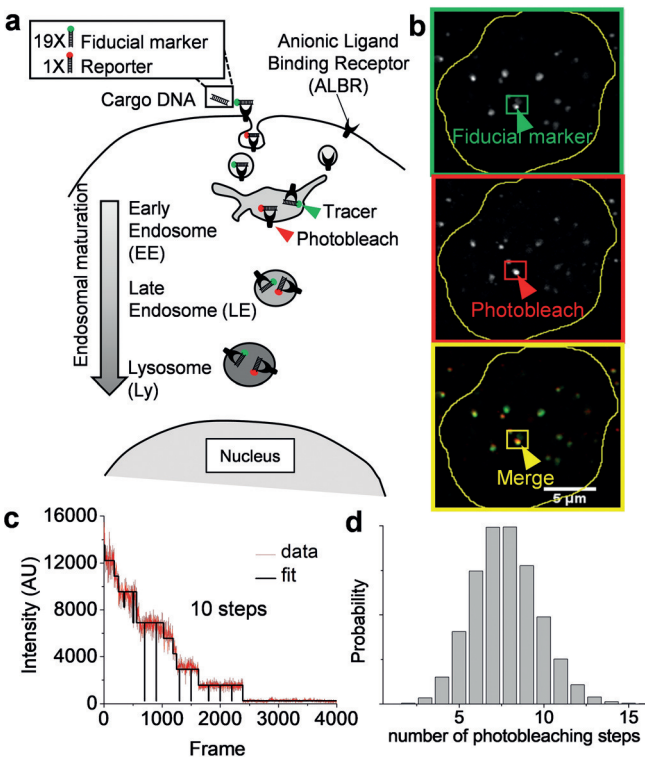

Figure 1. Work flow for counting the number of cargo DNA molecules in endosomes of J774 cells. a) Schematic of a cell labeled with a 19:1 ratio of dsDNA-A488 (fiducial marker)/dsDNA-Cy5 (reporter) along the endolysosomal pathway. b) Representative TIRF image of early endosomes (EE) of J774A.1 cells labeled with cargo DNA cocktail imaged in Alexa 488 channel and Cy5 channel. c) Representative photobleaching steps measured in Cy5 channel for the highlighted endosome. d) Histogram of number of photobleaching steps observed for $n = 200$ lysosomes. Number of devices per compartment = number of photobleaching steps observed × dilution factor.

endosomes ($n = 5$ cells), and 23% of lysosomes ($n = 5$ cells) were found to be illuminated. To eliminate artefacts arising from autofluorescence, only those compartments with both Alexa 488 and Cy5 signal were analyzed. Since both DNA probes have identical sequences, and scavenger receptors take up dsDNA mainly based on the overall negative charge,[17] uptake efficiency and organelle localization is expected to be similar, with all organelles showing similar ratios of Cy5/Alexa488 labels (Supporting Information, Figure S9). Cy5-labeled ssDNA was not retained in endosomes, either owing to its rapid degradation or endosomal translocation.[21] This worked in our favor, creating a clean system to report on the abundance of dsDNA cargo, which does not undergo endosomal translocation.[15] We then extracted the number of photobleaching steps for every Cy5 time-trace (Figure 1c and Supporting Information, Figure S7). The average number of DNA duplexes in a given compartment could then be calculated from the product of the number of photobleaching steps observed and the probe dilution factor, i.e., the ratio of dsDNA-A488 to dsDNA-Cy5 (Figure 1d).

To assign cargo DNA molecules to specific stages of endosomal maturation, we standardized pulse and chase times for cargo DNA to reach the early endosome, the late endosome, and the lysosome in J774A.1 cells. Using transferrin-rhodamine B as a marker for early/sorting endosomes,[19,20] we found maximal colocalization of transferrin-rhodamine B (500 nM) and cargo DNA (500 nM) in early endosomes (Figure 2a,d) and no colocalization in late endosomes and lysosomes for a 10 min pulse followed by a circa 5–10 min chase (Supporting Information, Figure S1). Similarly, ovalbumin marks late endosomes in J774A.1 cells.[8] We found significant cargo DNA colocalization with ovalbumin-FITC with a 10 min pulse and a 30 min chase, highlighting significant localization in late endosomes (Figure 2b,e) and insignificant colocalization in early endosomes and lysosomes (Supporting Information, Figure S2). Finally, for lysosomes, we used dextran-TMR, which is known to mark lysosomes in J774A.1 cells using a 16 h pulse and a 2 h chase. Cells treated with cargo DNA and labeled with dextran-TMR colocalized in lysosomes (Figure 2c,f) and the DNA cargo showed lack of colocalization in early and late endosomes (Supporting Information, Figure S3). Next, we established that extraneously added dsDNA was endocytosed specifically through the scavenger receptor (SR) pathway by using a competition assay.[17] We showed that Cy5-labeled cargo dsDNA (termed $I4_{Cy5}$) uptake was outcompeted by a 25-fold excess of maleylated BSA, which targets SRs (Figure 2g).

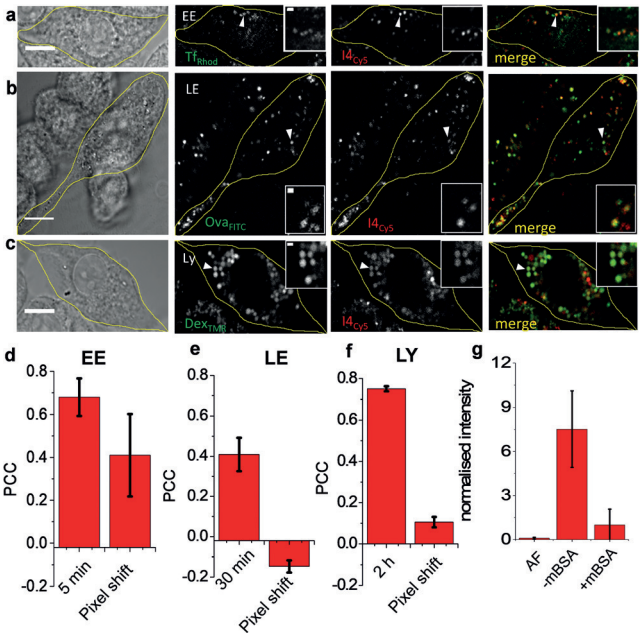

Figure 2. Representative single-plane confocal images showing co-localization of cargo with various compartment markers. J774A.1 cells were co-pulsed with dsDNA-Cy5 and a) EE/SE marker transferrin-rhodamine B (Tf_{Rhod}), b) LE marker ovalbumin-FITC (Ova_{FITC}), and c) lysosomal marker dextran-TMR (Dex_{TMR}) followed by 2 h chase. Cell boundaries are demarcated in yellow. d–f) Co-localization (Pearson's correlation coefficient, PCC) between cargo DNA and endosomal markers as a function of chase time in (a–c). Values indicate mean of $n \approx 20$ cells. g) $I4_{Cy5}$ internalization by J774A.1 cells in the presence (+mBSA) and absence (−mBSA) of excess competitor ligand maleylated BSA (mBSA, 10 µM) with autofluorescence control (AF). Error bars indicate the mean of independent experiments ± s.e.m. ($n = 30$ cells). Scale bars = 10 µm and 1 µm for inset.

Knowing the time-points of residence of cargo DNA at each stage along the endolysosomal pathway, we mapped cargo DNA abundance as a function of endosomal maturation (Supporting Information, Figure S4). We observed that early endosomes showed two kinds of populations, with endosomes containing circa 200 or circa 700 molecules. Overall, early endosomes showed a mean of 340 ± 60 cargo dsDNA molecules per endosome (Figure 3a, top, green line).

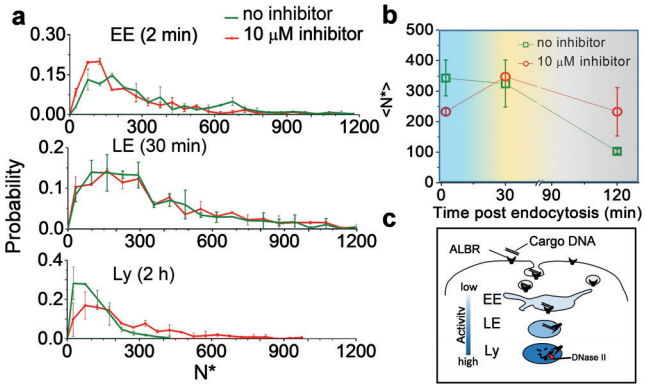

Figure 3. Quantitative maps of endosomal DNA processing by single molecule counting. a) Histograms of number of DNA devices observed per compartment in early endosomes (EE, 5 min post endocytosis), late endosomes (LE, 30 min post endocytosis), and lysosomes (Ly, 2 h post endocytosis) in presence and absence of 10 μM DNase II inhibitor within J774A.1 cells. b) Average number of DNA devices per compartment as a function of time. Blue indicates EE, orange indicates LE, and grey corresponds to Ly. Total number of devices per compartment (*N) = number of photobleaching steps observed × dilution factor. $n = 200$ endosomes (duplicate) c) Proposed model of DNase II activity in endosomes.

As DNA is endocytosed by clathrin-coated vesicles (ca. 100 nm), we speculate that the population of endosomes showing fewer cargo DNA molecules correspond to these smaller vesicles, while those endosomes showing larger amounts of cargo DNA could correspond to the larger sorting/early endosomes. Late endosomes revealed a fairly broad distribution of cargo DNA abundance with a mean of 320 ± 80 cargo dsDNA molecules per compartment (Figure 3a, middle, green line). Significantly, in lysosomes, the abundance of cargo DNA molecules showed an overall decrease, with most compartments having a mean of 103 ± 7 cargo DNA molecules, indicative of degradation or processing (Figure 3a, bottom, green line).

DNase II is known to be responsible for digestion of endocytosed DNA in macrophages. However, the specific endocytic organelle/s within which it is active is still unknown. To probe for organelle-specific activity of DNase II in immune cells, we treated the cells with a well-characterized specific peptide inhibitor of DNase II, ID2-3, and performed molecule counting experiments at each stage of endosomal maturation (Supporting Information, Figure S5). Upon treatment with a DNase II inhibitor, counting experiments on early endosomes revealed that the mean abundance of cargo dsDNA molecules in early endosomes decreased to 233 ± 12 upon DNase II inhibition (Figure 3b), suggesting a possible slowdown of endosomal maturation but not uptake. However, single endosome information on cargo abundances revealed that the population containing approximately 200 cargo dsDNA molecules had increased at the expense of the population containing approximately 700 cargo dsDNA molecules (P-value < 0.05). This suggests delayed endosomal maturation and homotypic fusion, as an overall decrease in DNA cargo owing to degradation was not observed. Further, cargo DNA abundance in late endosomes (LE) was not affected by DNase II inhibition (Figure 3a,b). Importantly, when we inhibited DNase II, we observed a significant accumulation of undigested cargo DNA in lysosomes (Ly), showing a mean centered at 230 ± 80 cargo DNA molecules (Figure 3a,b). Interestingly, our statistical data indicate that during DNase II inhibition, cells undergo reduced uptake/trafficking in the early endosomes (Supporting Information, Figure S8). This supports the current hypothesis[10] that DNase II-based endosomal DNA processing occurs mainly in lysosomes (Figure 3c).

Furthermore, delayed endosomal maturation as a result of cargo accumulation in lysosomes is also observed in the context of several lysosomal storage disorders, e.g., trafficking of acid sphingomyelinase (ASM) to the lysosome is impeded in ASM knock out cells owing to lysosomal accumulation of sphingomyelin.[24] Undigested DNA in endosomes of immune cells comprises one of many important triggers of the immune response. In mice, defective digestion of chromosomal DNA activates phagocytes, leading to anaemia in the embryo and chronic arthritis in adults.[25] Digestion of immunogenic CpG DNA in dendritic cells showed that endosomally localized DNase II activity is necessary to trigger TLR-9-mediated cytokine production.[4] Loss of DNase II activity results in autoimmune disorders such as systemic lupus erythomatosus, for which one of the hallmarks is the production of autoantibodies against dsDNA.[25,26] Our capacity to model the immune response using predictive computational models has been hindered by our inability to accurately specify the location and abundance of ligands such as dsDNA that trigger the immune response. The endosomal load of unprocessed dsDNA cargo is a function of the rate of endocytosis, concentration of exogenous dsDNA, receptor density on plasma membrane, and organelle-specific DNase II activity along the endolysosomal pathway.[4,27] Current methods to analyze DNA processing quantitate processing efficiency without organelle-specific information or organelle-specific information without the ability to quantitate processing.[28]

oSHiRLoC provides quantitative information on cargo DNA processing at organellar resolution. Endosomal cargo quantification using oSHiRLoC is not limited to dsDNA and can be applied to a range of externally added endocytic ligands. It can also be used to assay the location and activity of regulators of endosomal cargo processing. Given the burgeoning use of biologically active, synthetic DNA and RNA nanostructures and circulating endogenous DNA and RNA molecules, methods to understand their differential processing within the cell would be critical to uncover their mechanisms of action. The ability to determine the concentration of immunogens in specific endocytic organelles and correlate these with the strength of the downstream immune

response would enable us to quantitatively model the immune response.

Acknowledgements

We thank Shareefa Thekkan, Kasturi Chakraborty, Junyi Zou, Aditya Prakash, and Vytas Bindokas for technical assistance and code optimization and Research Computation Center (RCC) at the University of Chicago. We also thank Dr. Sethuramasundaram Pitchiaya, Damon Hoff, and Elizabeth Cameron for initial training. J774A.1 cells were a gift from Prof. Deborah Nelson, Department of Pharmacological and Physiological Sciences, the University of Chicago. S.P. acknowledges support from an NSF CAREER award.

Conflict of interest

The authors declare no conflict of interest.

Keywords: DNA · DNase II · lysosomes · photobleaching · single-molecule counting

How to cite: *Angew. Chem. Int. Ed.* **2019**, *58*, 3073 – 3076
Angew. Chem. **2019**, *131*, 3105 – 3108

[1] M. Rincon-Restrepo, A. Mayer, S. Hauert, D. K. Bonner, E. A. Phelps, J. A. Hubbell, et al., *Biomaterials* **2017**, *132*, 48 – 58.
[2] G. M. Barton, J. C. Kagan, R. Medzhitov, *Nat. Immunol.* **2006**, *7*, 49 – 56.
[3] E. B. Compeer, T. W. H. Flinsenberg, S. G. van der Grein, M. Boes, *Front. Immunol.* **2012**, *3*, 37.
[4] M. P. Chan, M. Onji, R. Fukui, K. Kawane, T. Shibata, S. Saitoh, et al., *Nat. Commun.* **2015**, *6*, 5853.
[5] M. Amessou, V. Popoff, B. Yelamos, A. Saint-Pol, L. Johannes, *Curr. Protoc. Cell Biol.* **2006**, *32*, 15.10.1 – 15.10.21.
[6] A. Weihe, *Methods Mol. Biol.* **2014**, *1132*, 235 – 243.
[7] J. J. Sperinde, S. J. Choi, F. C. Szoka, *J. Gene Med.* **2001**, *3*, 101 – 108.
[8] T. E. Tjelle, A. Brech, L. K. Juvet, G. Griffiths, T. Berg, *J. Cell Sci.* **1996**, *109*, 2905 – 2914.
[9] Z. Qian, P. G. Dougherty, D. Pei, *Chem. Commun.* **2015**, *51*, 2162 – 2165.
[10] C. J. Evans, R. J. Aguilera, *Gene* **2003**, *322*, 1 – 15.
[11] J. A. Brown, R. T. Swank, *J. Biol. Chem.* **1983**, *258*, 15323 – 15328.
[12] J. Yang, H. Chen, I. R. Vlahov, J.-X. Cheng, *Proc. Natl. Acad. Sci. USA* **2006**, *103*, 13872 – 13877.
[13] E. M. Puchner, J. M. Walter, R. Kasper, B. Huang, W. A. Lim, *Proc. Natl. Acad. Sci. USA* **2013**, *110*, 16015 – 16020.
[14] R. Jungmann, M. S. Avendaño, M. Dai, J. B. Woehrstein, S. S. Agasti, Z. Feiger, et al., *Nat. Methods* **2016**, *13*, 439 – 442.
[15] K. Tsekouras, T. C. Custer, H. Jashnsaz, N. G. Walter, S. Pressé, *Mol. Biol. Cell* **2016**, *27*, 3601 – 3615.
[16] S. Pitchiaya, L. A. Heinicke, J. I. Park, E. L. Cameron, N. G. Walter, *Cell Rep.* **2017**, *19*, 630 – 642.
[17] S. Modi, M. G. Swetha, D. Goswami, G. D. Gupta, S. Mayor, Y. Krishnan, *Nat. Nanotechnol.* **2009**, *4*, 325 – 330.
[18] S. Surana, J. M. Bhat, S. P. Koushika, Y. Krishnan, *Nat. Commun.* **2011**, *2*, 340.
[19] N. Narayanaswamy, K. Chakraborty, A. Saminathan, E. Zeichner, K. Leung, J. Devany, Y. Krishnan, *Nat. Methods* **2019**, *16*, 95 – 102.
[20] S. Thekkan, M. S. Jani, C. Cui, K. Dan, G. Zhou, L. Becker, Y. Krishnan, *Nat. Chem. Biol.* **2018**, https://doi.org/10.1038/s41589-018-0176-3.
[21] S. Lorenz, S. Tomcin, V. Mailänder, *Microsc. Microanal.* **2011**, *17*, 440 – 445.
[22] C. I. Raje, S. Kumar, A. Harle, J. S. Nanda, M. Raje, *J. Biol. Chem.* **2007**, *282*, 3252 – 3261.
[23] S. J. Wadsworth, H. Goldfine, *Infect. Immun.* **2002**, *70*, 4650 – 4660.
[24] R. Dhami, E. H. Schuchman, *J. Biol. Chem.* **2004**, *279*, 1526 – 1532.
[25] K. Kawane, H. Fukuyama, G. Kondoh, J. Takeda, Y. Ohsawa, Y. Uchiyama, et al., *Science* **2001**, *292*, 1546 – 1549.
[26] K. Kawane, K. Motani, S. Nagata, *Cold Spring Harbor Perspect. Biol.* **2014**, *6*, a016394.
[27] C. C. Scott, F. Vacca, J. Gruenberg, *Cell Dev. Biol.* **2014**, *31*, 2 – 10.
[28] N. Hiroi, V. M. Draviam, A. Funahashi, *Front. Physiol.* **2016**, *7*, 196.

Manuscript received: October 16, 2018
Revised manuscript received: January 1, 2019
Accepted manuscript online: January 22, 2019
Version of record online: February 5, 2019

